Chemical Science

ROYAL SOCIETY OF CHEMISTRY

EDGE ARTICLE

View Article Online
View Journal | View Issue

Cite this: *Chem. Sci.*, 2023, **14**, 2990

All publication charges for this article have been paid for by the Royal Society of Chemistry

Stille type P–C coupling polycondensation towards phosphorus-crosslinked polythiophenes with P-regulated photocatalytic hydrogen evolution†

Zhikai Zhang, ‡ Boyang Zhang, ‡ Xue Han,‡ Hongyi Chen, Cece Xue, Min Peng, Guijun Ma * and Yi Ren *

Received 6th December 2022
Accepted 13th February 2023

DOI: 10.1039/d2sc06702a

rsc.li/chemical-science

Recently, exploring new type polymerization protocols has been a major driving force in advancing organic polymers into highly functional materials. Herein we report a new polycondensation protocol to implant the phosphorus (P) atom in the main backbone of crosslinked polythiophenes. The polycondensation harnesses a Stille phosphorus–carbon (P–C) coupling reaction between phosphorus halides and aryl stannanes that has not been reported previously. Mechanistic studies uncovered that the P-electrophile makes the reactivity of a catalytic Pd-center highly sensitive towards the chemical structures of aryl stannanes, which is distinct from the typical Stille carbon–carbon coupling reaction. The efficient P–C polycondensation afforded a series of P-crosslinked polythiophenes (PC-PTs). Leveraging on the direct P-crosslinking polymerization, solid-state ^{31}P NMR studies revealed highly uniform crosslinking environments. Efficient post-polymerization P-chemistry was also applied to the PC-PTs, which readily yielded the polymers with various P-environments. As a proof of concept, new PC-PTs were applied as the photocatalysts for H_2 evolution under visible light irradiation. PC-PTs with an ionic P(Me)-center exhibit a H_2 evolution rate up to 2050 μmol h^{-1} g^{-1}, which is much higher than those of PC-PTs with a P(O)-center (900 μmol h^{-1} g^{-1}) and P(III)-center (155 μmol h^{-1} g^{-1}). For the first time, the studies reveal that regulating P-center environments can be an effective strategy for fine tuning the photocatalytic H_2 evolution performance of organic polymers.

Introduction

Organic π-conjugated polymers (OCPs) have attracted much attention in both academics and industries.[1–6] Due to diverse chemical structures and properties, OCPs have been successfully applied to the areas of organic catalysis, optoelectronics, bio-imaging/sensing, and energy conversion.[1–6] The functionalities of OCPs are highly dictated by the distinct chemical structures of the building blocks.[1–11] Recently, introducing main-group elements (such as B, N, S, Si, P, *etc.*) into polymeric backbones has become a powerful strategy for fine-tuning photophysics, redox characteristics, molecular organizations, and optoelectronic functionalities of the OCPs.[12–18] For example, embedding boron (B)-building blocks into OCPs induced a strong p–π* electronic coupling between B and polymeric backbones, which endowed the polymers with excellent toxic chemical (fluoride, cyanide, and amines) sensing properties, electron-transporting properties, and electron-accepting properties.[12,19–22] The introduction of sulfone (SO_2)-containing units enhanced the electron-accepting character and water affinity of OCPs, which afforded new polymeric systems with excellent photocatalytic H_2 evolution performance.[23–26]

Phosphorus (P) is a special member of the main-group elements. P-containing species exhibit widespread applications in drug design,[27] life science,[28] synthetic chemistry,[29–33] and materials chemistry.[34,35] Recently, doping various kinds of P-centers into building blocks, such as P(III)-, P(O)-, P(metal)-, and P(Me)-centers, has been demonstrated to be an effective strategy to fine-tune optoelectronic properties of OCPs.[36–40] However, these diverse P-building blocks, particularly P(III) and cationic P(Me) derivatives generally involved multi-step synthesis and problematic purification processes. Therefore, we envisioned that using the simple and commercially available phosphorus halides as the polymerization starting material is more appealing for considerably streamlining the synthesis and diversifying the chemical structure of OCPs. Research on transition-metal (TM) catalyzed phosphorus–carbon (P–C) formations has witnessed a significant development in the fields mentioned above.[41–45] However, TM catalyzed arylation of phosphorus halides is still less studied in the literature.[41–45] To the best of our knowledge, research on TM-catalyzed triple

School of Physical Science and Technology, ShanghaiTech University, Shanghai 201210, China. E-mail: renyi@shanghaitech.edu.cn; magj@shanghaitech.edu.cn

† Electronic supplementary information (ESI) available. See DOI: https://doi.org/10.1039/d2sc06702a

‡ These authors contributed equally.

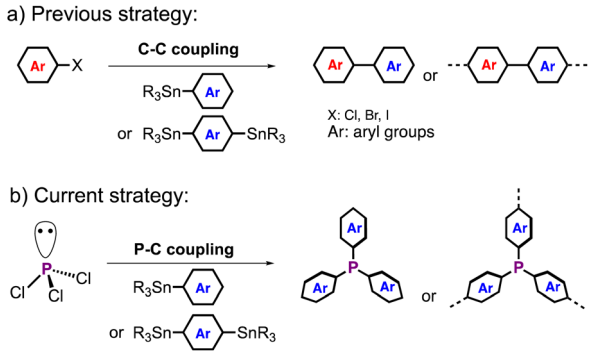

Scheme 1 (a) Previous polymerization strategy *via* a Stille C–C coupling reaction and (b) new polymerization strategy *via* a Stille P–C coupling reaction in this study.

arylations at a single P-center has not been reported in the literature.

Herein we report a new type of Stille phosphorus–carbon (P–C) polycondensation between PCl_3 and aryl stannanes, in which the triple P–C bond formation at a single P-center can be achieved under optimized conditions (Scheme 1). Small molecule studies and mechanistic studies uncovered a distinct P-effect in the coupling reaction. The efficient P–C heterogeneous polycondensation afforded a new series of P-crosslinked polythiophenes (PC-PTs). Solid-state ^{31}P (ss)NMR spectroscopy experiments revealed highly uniform crosslinked P-centers. Further applying post-polymerization P-chemistry, such as oxidation and methylation, gave new PC-PTs with various better-controlled P-centers. As a proof of concept, PC-PTs act as good photocatalysts for hydrogen (H_2) production in aqueous solutions.

Results and discussion

Due to efficient reactivity and facile preparation procedures, the Stille C–C coupling reaction has been widely used for the preparation of functional OCPs.[46–48] With the well-documented low-energy σ*-orbital of phosphorus–halide (P–X) bond in phosphorus halides,[35] we expected that the oxidative addition of the P–X bond to Pd(0) would readily occur as that in the typical Stille coupling reaction. When having the appropriate nucleophiles, such as aryl stannanes, in the catalytic system, transmetallation and subsequent reductive elimination would take place to afford the product and complete the catalytic cycle. Therefore, it is highly possible that the typical Stille coupling is applicable to P–C bond formation for synthesizing P-OCPs. Although P–C bonds can form by using organometallic reagents, such as organolithiums and Grignard reagents in small-molecule synthesis, the highly reactive nucleophilic character and weak stability in some organic solvents (such as tetrahydrofuran) of the organometallic reagents make them less practical in the synthesis of P-OCPs with high yields and uniform structures.

With the well-established chemical modifications and diverse optoelectronic properties,[1,5,15,49,50] we expected that doping tunable P-environments will offer us with an efficient

Table 1 Optimization of the reaction between PCl_3 and ThSn under various reaction conditions[a]

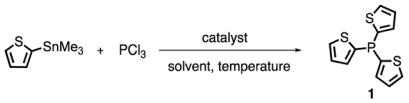

Entry	Catalyst	Solvent	Temperature (°C)	Yield[b] (%)
1	None	Toluene	100	0
2	$Ni(acac)_2$	Toluene	100	82(80)
3	$Ni(dppp)Cl_2$	Toluene	100	90(86)
4	$Pd(PPh_3)_4$	Toluene	100	68(67)
5	$Pd(PPh_3)_2Cl_2$	Toluene	100	67(66)
6	$Pd_2(dba)_3$	Toluene	100	74(74)
7	$Pd(OAc)_2$	Toluene	100	93(90)
8	$Pd(OAc)_2$	Toluene	r.t.	31(29)
9	$Pd(OAc)_2$	Toluene	70	73(73)
10	$Pd(OAc)_2$	Toluene	120	81(80)
11	$Pd(OAc)_2$	Chlorobenzene	100	95(95)
12	$Pd(OAc)_2$	*o*-DCB	100	89(88)
13[c]	$Pd(OAc)_2$	Toluene	100	96(90)

[a] Reaction conditions: PCl_3 (0.5 mmol, 1.0 eq), ThSn (1.875 mmol, 3.75 eq), catalyst (0.025 mmol, 0.05 eq) and solvent (1 mL), 24 h under N_2. [b] Determined by quantitative ^{31}P NMR (isolated yields in parentheses). [c] PBr_3 used as an alternative to PCl_3.

strategy to fine-tune the optoelectronic properties of the doped polythiophenes. First, we tested the small-molecule reaction between PCl_3 and trimethyl(thiophen-2-yl)stannane (ThSn) to optimize the reaction conditions for polycondensation. Table 1 shows the model reaction under various conditions. Without catalysts, the reaction does not afford the target trisubstituted product **1** even at 100 °C, and only monosubstituted product was observed (Table 1, entry 1). In the presence of various Pd or Ni catalysts, product **1** can be obtained in good yields (Table 1, entries 2–7). Particularly, 93% yield of **1** can be obtained using $Pd(OAc)_2$ as the catalyst. We also optimized the reaction temperature (Table 1, entries 7–10). The results show that the reaction using $Pd(OAc)_2$ at 100 °C gave the best yield of **1**. Besides, using chlorobenzene (CB) and 1,2-dichlorobenzene (*o*-DCB) as solvents does not significantly affect the product yields (Table 1, entries 11 and 12). The P–C coupling reaction is also applicable to PBr_3 as the starting material (Table 1, entry 13), in which a 96% yield of **1** was obtained.

We also tested the compatibility of the P–C coupling reaction towards various aryl substrates. Surprisingly, when using trimethyl(phenyl)stannane (PhSn) as the substrate, a low yield of product **2** (0.4%) was obtained (Scheme 2). Furthermore, the presence of either electron-withdrawing or electron-donating substituents on the phenyl group does not significantly improve product yields (**3**: 12%, **4**: 12%, **5**: 0%, and **6**: 16%, Scheme 2).

In order to reveal the different reactivity of aryl stannanes in the coupling reactions, we carried out theoretical studies by using ThSn and PhSn as the representative aryl stannanes. Previous mechanistic studies of the Stille C–C coupling reaction provided a base for the possible mechanism of the P–C coupling

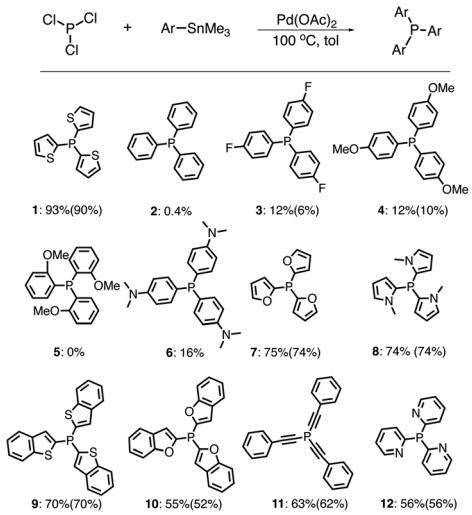

Scheme 2 P–C coupling reactions between PCl_3 and various aryl stannanes (Quantitative ^{31}P NMR yields given below and isolated yields given in parentheses).

reaction.[46–54] The plausible reaction pathway is shown in Fig. 1a. We also calculated the free energy changes by using density functional theory (DFT) calculations (see the details in the ESI†). Due to the large excess of PCl_3 used in the reactions, PCl_3 was considered as the ligand in the catalytic process. The catalytic reaction starts with the oxidative addition of the P–Cl bond to Pd(0).[55] The oxidative addition is an exergonic process, which affords **3c** with a *cis*-structure. The calculations show that the maximum barrier height (10.5 kcal mol^{-1}) for the transition state **TS1** of the reaction pathway occurs for the oxidative addition step. As suggested in previous studies of Stille C–C coupling reactions,[52] **3c** further undergoes a structural isomerization to **3t** with a *trans*-structure.

In transmetallation, ThSn and PhSn exhibit different coordination strength towards the Pd center of **3t**. The Pd–C distances of intermediate **4Th** (2.253 Å and 2.923 Å) are shorter than those of **4Ph** (2.460 Å and 2.978 Å) (Fig. 1b), which is in line with the slightly lower energy of **4Th**. The difference is more pronounced in the transition state. The formation of **TS2Th** with ThSn is endergonic by +2.1 kcal mol^{-1}. The formation of **TS2Ph** with PhSn is more endergonic by +2.7 kcal mol^{-1}. In the transition state, **TS2Th** ($\Delta G^{\ddagger}$ = 4.5 kcal mol^{-1}) having a more product like structure exhibits a lower energy barrier compared with that of **TS2Ph** ($\Delta G^{\ddagger}$ = 6.0 kcal mol^{-1}) (Fig. 1a and b). The lower energy barrier of **TS2Th** is consistent with the higher yield of the P–C coupling when using ThSn as the nucleophile.

To further reveal the different reactivity, we also calculated the Mulliken charge of the Pd center in **3t**. When compared with that of **3t′** (1.05) in the oxidation between phenyl chloride and **1**, the Mulliken charge of the Pd center in **3t** (0.33) is significantly less positive (Fig. 1a). The comparison between **3t** and **3t′** clearly suggests that the Pd-center of **3t** is less electrophilic compared with that of **3t′**. According to the theoretical study, it is rationalized that the electron-rich P-center of the PCl_2 group weakens the electrophilic character of the Pd center. The P–C coupling reaction with the weakened Pd-center is very distinct from the typical Stille C–C coupling reaction. The weak electrophilic character probably makes the reactivity of the coupling reaction highly sensitive to the nucleophilic character of aryl stannanes in the transmetallation process.

Compared with PhSn, strong nucleophilic aryl stannanes with a similar size are expected to be more kinetically favorable to undergo the transmetallation process.[56,57] Consistent with our theoretical hypothesis, the P–C coupling reactions worked well when using trimethyl(furan-2-yl)stannane, 1-methyl-2(trimethylstannyl)-1*H*-pyrrole, and 2-(trimethylstannyl)pyridine as the nucleophiles (**7**, **8**, and **12** in Scheme 2). With the weakened Pd center of **3t**, aryl stannanes with larger size are also expected to be kinetically less reactive in the coupling reactions. Consistently, using benzo[*b*]thiophen-2-yl(trimethylstannane), benzofuran-2-yl(trimethylstannane), and trimethyl(phenylethynyl) stannane with the larger size aryl substituents gave lower yields of trisubstituted products (**9**, **10**, and **11** in Scheme 2) compared with that of the coupling reaction using ThSn under similar conditions.

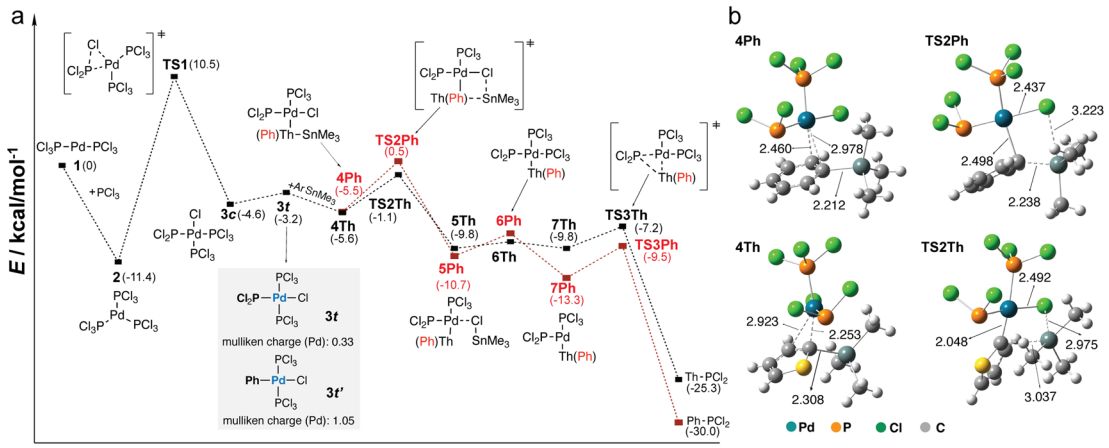

Fig. 1 (a) Computational studies of the P–C coupling reactions computed at the SMD (toluene)-B3LYP-D3/6-311+G(d)&SDD//B3LYP/6-31G(d) &SDD level. (b) Optimized structures of **4Ph**, **4Th**, **TS2Ph**, and **TS2Th** (bond length in Å).

After transmetallation with aryl stannanes, subsequent reductive elimination would take place to afford the product and complete the catalytic cycle (Fig. 1a). It is worth mentioning that the purpose of exploring the various substrates is to support the theoretical studies and identify the broad compatibility of the P–C coupling reaction, and not to fully optimize the reaction conditions for each substrate. According to the large number of references referring to optimizations of Stille C–C coupling reactions,[46–54] it is reasonable to believe that further reaction optimizations, such as catalyst–ligand systems, additives (CsF, CuI, *etc.*), solvents, and temperature could improve the yields of the reactions with various substrates. Previously, Stille and coworkers reported similar Pd-catalyzed coupling between stannyl/silyl phosphine reagents and aryl halides.[58] Different from the previous work where the P-reagents act as nucleophiles in the coupling, PCl_3 acts as an electrophile in the current coupling. Furthermore, efficient multiple P–C bond formation in a single P-center was not reported in the previous study.

Encouraged by the efficient P–C coupling reactions, we explored the coupling reaction in crosslinked polycondensation. Previous study has shown that triaryl P-building blocks with a P(III) center may undergo quaternization in the presence of Pd(0) catalysts.[37] The fact that similar quaternization of the P-center is not observed in our P–C coupling reaction is beneficial for synthesizing P-OCPs with a uniform P(III)-center. We chose distannylated oligothiophenes (**B1**, **B2**, and **B3**) as co-polymerization building blocks, due to the high reaction yield of stannylated thiophenes under the current conditions. Initially, polycondensations between PCl_3 and distannylated oligothiophenes were carried out at 100 °C in toluene, which afforded an incomplete P-crosslinking environment based on the solid-state ^{31}P (ss)NMR experiment. Therefore, the polycondensations were carried out at an elevated temperature (160 °C in *o*-DCB) to give **P1**, **P2**, and **P3** (Scheme 3). We conducted ^{31}P and ^{13}C ssNMR spectroscopy experiments, Fourier transform infrared (FTIR) spectroscopy experiments, and X-ray photoelectron spectroscopy (XPS) experiments to characterize chemical structures of the crosslinked polymers (see details in the ESI†).

The direct P–C crosslinking polymerization allows ^{31}P ssNMR experiments to unambiguously reveal the crosslinking environments of PC-PTs. According to the ^{31}P NMR signal of small molecule tri(thiophen-2-yl)phosphane (**1**: −46.2 ppm), strong ^{31}P ssNMR signals of **P1** (−44.2 ppm), **P2** (−41.9 ppm), and **P3** (−42.3 ppm) are assigned to the P(III)-environment (Fig. 2a). The presence of one main strong ^{31}P signal suggests that most P-centers are fully crosslinked in the polymeric networks synthesized by the heterogeneous polycondensation.

We also synthesized the related polymer **P2′** with the same bithiophene building block as **P2**, in which dilithiated bithiophene was used as the monomer in an alternative protocol (Scheme 3). Different from that of **P2**, the ^{31}P ssNMR spectrum of **P2′** shows multiple ^{31}P signals, indicating a less uniform P-environment (Fig. 2a). In the FTIR spectrum, we observed a strong broad signal at 3380 cm^{-1} (Fig. S8c†), which is likely due to the presence of the P–OH group in **P2′**. In a previous study, P-porous organic polymers synthesized by a similar lithiation method also display a similar broad signal in the range of 3400–3500 cm^{-1}, which was attributed to the P–OH groups.[59] We rationalized that the lithiation mediated polycondensation resulted in high content of not fully substituted P-centers, such as $RPCl_2$ and R_2PCl. Although **P2′** was handled and stored under inert gas conditions, the highly reactive $RPCl_2$ and R_2PCl groups likely hydrolyzed to give the

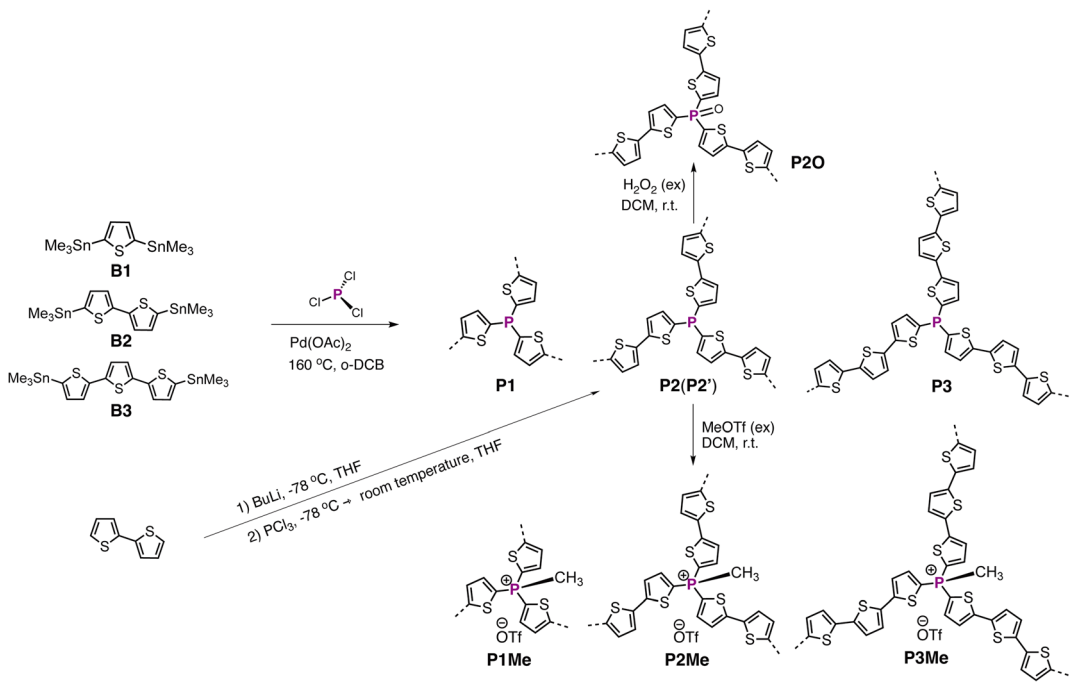

Scheme 3 P–C polycondensation and post-methylation and oxidation of PC-PTs.

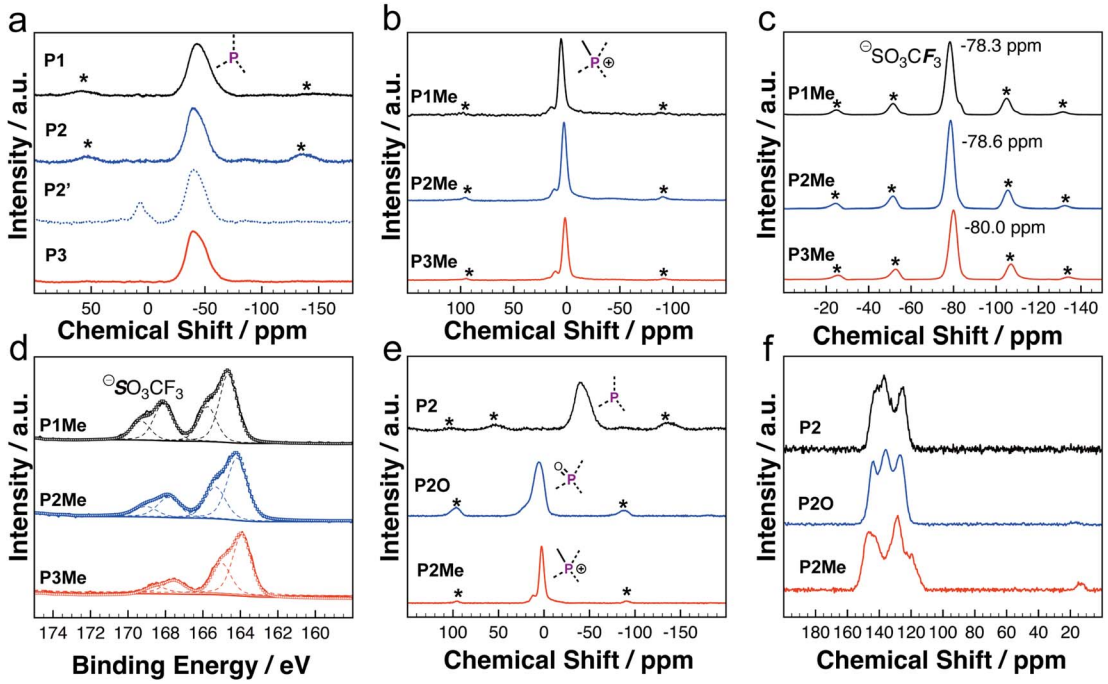

Fig. 2 (a) ^{31}P HPDEC/MAS NMR spectra of **P1**, **P2**, and **P3**. (b) ^{31}P HPDEC/MAS NMR spectra, (c) ^{19}F MAS NMR spectra, and (d) XPS spectra in the S 2p region of **P1Me**, **P2Me**, and **P3Me**. (e) ^{31}P HPDEC/MAS NMR spectra and (f) ^{13}C CP/MAS NMR spectra of **P2**, **P2O**, and **P2Me** (asterisks represent sidebands).

P–OH group during the workup or ^{31}P ssNMR and FTIR measurements. Under similar conditions, the FTIR spectrum of **P2** does not show a noticeable signal in a similar range (Fig. S8†). Even after the oxidation reaction in H_2O_2 (30% aqueous solution), the FTIR spectrum of **P2O** does not show a noticeable signal in the range of 3400–3500 cm^{-1} (Fig. S7†). The results suggest that the Pd-catalyzed P–C polycondensation is more suitable for constructing PC-PTs compared with the lithiation mediated polycondensation, in which the P–C polycondensation afforded PC-PTs with a better controlled and uniformly crosslinked P-center.

We further conducted heterogeneous methylation chemistry on PC-PTs (Scheme 3, see the details in the ESI†). Compared with those of **P1**, **P2**, and **P3**, ^{31}P ssNMR spectra of **P1Me** (5.2 ppm), **P2Me** (2.6 ppm) and **P3Me** (1.5 ppm) exhibit clear downfield chemical shifts (Fig. 2b), which are consistent with ^{31}P NMR chemical-shift changes observed in related P(Me)-containing oligothiophenes.[60] Moreover, the observations of the peaks at *ca.* 79–80 ppm in ^{19}F ssNMR spectra (Fig. 2c), the peaks at *ca.* 13–14 ppm in ^{13}C ssNMR spectra (Fig. 2f and S1–S3†), and the new sulfur peaks between 166 and 170 eV in XPS spectra (Fig. 2d) are consistent with the presence of both the P(Me)-center and OTf counter anion in **P1Me**, **P2Me** and **P3Me**. The results revealed that the heterogeneous methylation is highly efficient in PC-PTs. In XPS experiments, element ratios of all the PC-PTs are close to the theoretical values (Table S3†). Thermogravimetric (TGA) experiments (Fig. S13†) showed that all the PC-PTs show a weight loss of 5% under a nitrogen atmosphere above 250 °C.

With well-characterized PC-PTs in hand, we explored their potential applications in photocatalytic H_2 evolution. Although OCPs have become promising organic photocatalysts for H_2 evolution, P-OCPs are still under developed in the field.[61–64] To the best of our knowledge, OCPs with an ionic P(Me) center have not been explored in the field of photocatalytic H_2 evolution. We tested the photocatalytic H_2 evolution activities of **P2Me** and **P3Me** as the representative polymers, using ascorbic acid (AC) as a sacrificial electron donor (SED) and Pt as a co-catalyst in aqueous solutions. The photocatalytic results (Fig. 3a) revealed that the normalized hydrogen evolution rates (HERs) under full-arc illumination of **P2Me** and **P3Me** are 3200 μmol h^{-1} g^{-1}, and 1750 μmol h^{-1} g^{-1}, respectively. **P2Me** and **P3Me** also exhibit photocatalytic H_2 evolution under visible light (λ > 420 nm) (Fig. 3b), in which **P2Me** and **P3Me** exhibit the HERs of 2050 μmol h^{-1} g^{-1} and 800 μmol h^{-1} g^{-1}, respectively. The exact reason for the better performance of **P2Me** is still unclear at the moment. Previous studies revealed that increasing the number of thiophene units increased the ionization potential (IP) of thiophene-based polymers, which suppresses the oxidation of the SED, and consequently influences the overall HERs.[26,61,64] A similar explanation may also be applicable to our systems in the current study.

The rich and well-defined P-environments in the PC-PT networks encouraged us to further investigate the impacts of P-chemistry on the photocatalytic performance, which has not been discussed in the literature. Due to the better photocatalytic performance, we investigated the P-effects by using the **P2** series as the representatives. A dispersion of **P2** and an excess of H_2O_2 in dichloromethane (DCM) solution was stirred for 24 hours at room temperature (Scheme 3), which afforded **P2O** in high yield (99%). In Fig. 2e, the ^{31}P ssNMR spectrum of **P2O** (5.9 ppm) shows a downfield chemical-shift compared to that of **P2** (−42

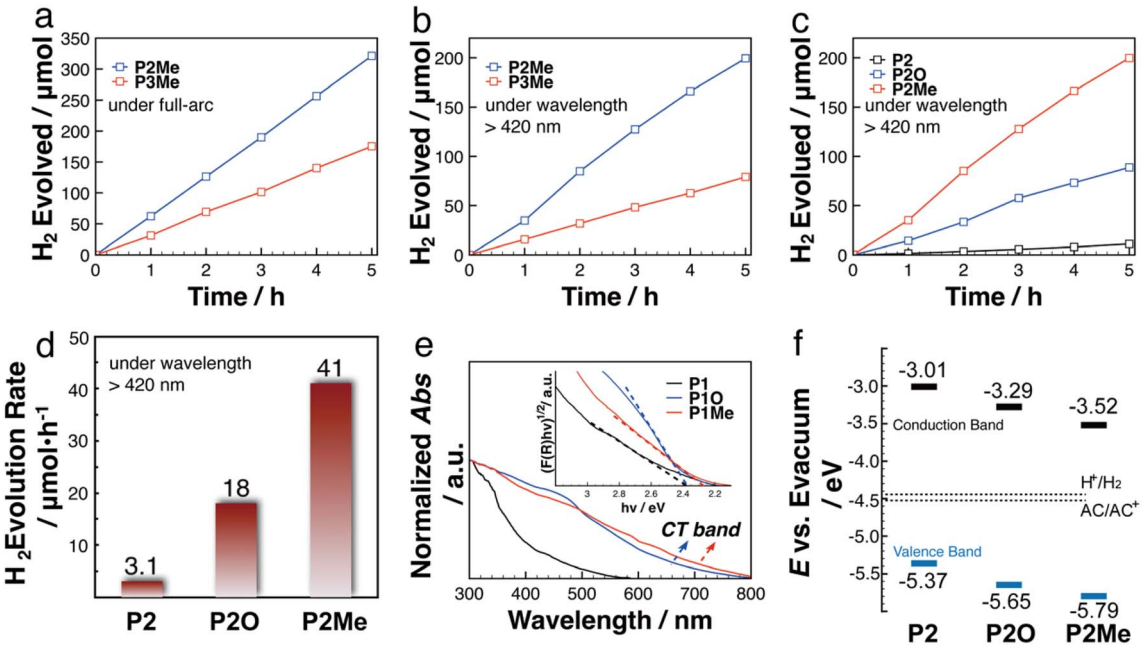

Fig. 3 (a) Time course for photocatalytic H_2 evolution under full-arc and (b) $\lambda > 420$ nm light illumination using 20 mg of photocatalysts **P2Me** and **P3Me**. (c) Time course for photocatalytic H_2 evolution, (d) photocatalytic H_2 evolution rates, (e) solid-state UV-vis diffuse reflectance spectra (Tauc plot), and (f) band structure diagram of the **P2** series.

ppm), which is in line with the oxidation of the P-center. The detailed characterization of **P2O** is shown in the ESI.† As shown in Fig. 3c and d, HERs of the **P2** series polymers exhibit a strong correlation with the P-environments, in which the HERs gradually increase from **P2** with a P(III)-center (155 μmol h^{-1} g^{-1}), over **P2O** with a P(O)-center (900 μmol h^{-1} g^{-1}), to **P2Me** with a P(Me)-center (2050 μmol h^{-1} g^{-1}). It is noticeable that the HER of **P2** is five times higher than that of **P2′** (Fig. S8d†), which highlights the impact of better controlled P-crosslinking centers on the photocatalytic performance.

To shed light on the P-effect, we conducted experimental and theoretical studies on the polymers. As shown in Fig. 3e, **P2O** and **P2Me** exhibit weak low-energy absorption bands (between 500 nm and 800 nm), which are tentatively assigned to the intramolecular charge transfer (ICT) band (*vide infra*). Compared with that of **P2**, the broader and red-shifted absorption spectra of **P2O** and **P2Me** are beneficial for the better photocatalytic performances under visible light.

We calculated the conduction band (CB) minimum energy levels of the **P2** series based on the Mott–Schottky experiments. Combined with the UV-vis diffuse reflectance data, we are able to plot the relative positions of the CB and valence band (VB) of the **P2** series (Fig. 3f). Compared to the reduction potential of H^+ (−4.44 eV), the higher CBs of **P2** (−3.01 eV), **P2O** (3.29 eV), and **P2Me** (−3.52 eV) are thermodynamically favourable for the intermolecular electron transfer from the **P2** series to H^+. Previous studies also revealed that the HERs of OCP photocatalysts correlated with not only the reduction of H^+, but also the oxidation of the SED.[23–26,61,62] The reluctant oxidation of SEDs has been demonstrated to result in low HERs of photocatalytic H_2 evolution in some systems, in which the oxidation is the rate determination step.[26,58,59] In our case, the lower VB of **P2Me** (−5.79 eV) may provide a stronger driving force for the oxidation of the SED compared with **P2** (−5.37 eV) and **P2O** (−5.65 eV), thus playing positive roles in the photocatalytic performance.

Previously, the wettable sulfone group is also believed to be responsible for the accelerated charge and proton transfer at the interface between polymer backbones and water molecules.[23,26,65] The hydrophilic nature of the ionic P(Me)-center is supported by the lower contact angles of water droplets on **P2Me** (39°) compared with **P2O** (61°) and **P2** (74°) (Fig. S20†). Therefore, the highly wettable P(Me)-group of **P2Me** may act similarly as the sulfone group in the photocatalytic process.

To further better understand the P-effects on the photocatalytic performances of the **P2** series, we also conducted the theoretical studies of model compounds (Fig. 4). The structures of the 1st generation model compounds were optimized at the level of RCAM-B3LYP/6-31G(D). TD-DFT at the level of RCAM-B3LYP/6-31G(D) scrf = (solvent = dichloromethane) was employed for the energy calculations (see the details in the ESI†). Both HOMO and LUMO energy levels decrease gradually from **M**, over **MO** to **MMe**, which are in line with the trends observed in the VB and CB. The decreased HOMO and LUMO energy levels can be attributed to the enhanced electron-withdrawing effect from the P(III)-center, over the P(O)-center to the P(Me)-center. Furthermore, compared to those of **M** and **MO**, frontier molecular orbitals (FMOs) of **MMe** show a noticeable intramolecular charge transfer (ICT) character (Fig. 4). When switched to the larger model molecules, the 2nd generation model molecules consistently exhibit narrower HOMO–LUMO gaps. Again, both HOMO and LUMO energy levels decrease gradually from **M2**, over **M2O**,

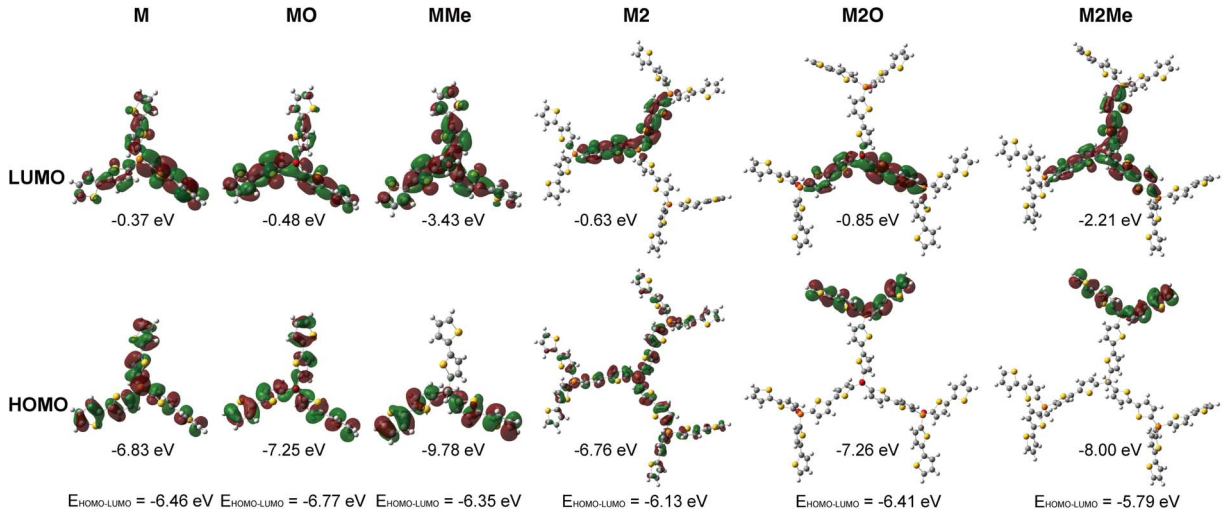

Fig. 4 FMOs of the 1st generation (**M**, **MO**, and **MMe**) and the 2nd generation (**M2**, **M2O**, and **M2Me**) model molecules.

to **M2Me**. Compared to the 1st generation model molecules, all the 2nd generation model molecules show noticeable ICT character (Fig. 4 and Table S3†). Particularly, **M2O** and **M2Me** show a stronger charge separation (CS) characteristic where the HOMO and LUMO display almost zero overlap. According to previous studies,[62,63,66] the strong intramolecular CS character and lowered HOMO of P(Me)-PTs revealed in the theoretical studies could play a beneficial role in achieving efficient photocatalytic H_2 evolution.

Our studies suggest that the balanced FMO energy level, better wettability, and strong ICT character are strongly dependent on the P-environments, which work collaboratively to give the better photocatalytic process of **P2Me** compared with its counterparts. With the characteristics of efficient polymerization and better-controlled chemical modification, doping an ionic P(Me)-center into polymeric backbones is a promising strategy for constructing OCPs with excellent photocatalytic H_2 production. Although the preliminary photocatalytic results do not outperform the best OCPs in the field, the strong impact of P-chemistry on the photocatalytic performances reminds us of the most employed sulfone (SO_2) group in the OCP photocatalysts.[23,26,67] With the extensive optimization, the HERs of SO_2-OCPs continue to increase where a HER up to 9772 μmol h^{-1} g^{-1} has been obtained recently.[23,26,67] **P2Me** exhibits a comparable HER to that of the first generation of SO_2-OCPs (600–3000 μmol h^{-1} g^{-1}).[68] Therefore, we believe that the photocatalytic performances of P(Me)-OCPs could be further improved by judicious optimization of the polymeric catalyst systems in the future.

Conclusions

In summary, we report a new type of Stille P–C polycondensation, in which efficient multiple P–C bond formation can be achieved at a single P-center. The mechanistic studies of small molecules uncovered the significantly weakened electrophilic character of the Pd center due to the P-effect, which is different from the typical Stille coupling reaction. Furthermore, the highly efficient P–C polycondensation and well-controlled post-polymerization P-chemistry provided a good platform for constructing new PC-PT networks with better-controlled/-defined P-environments. We further applied PC-PTs as photocatalysts for H_2 production. Our preliminary results uncovered, for the first time, that fine-tuning the environments of P-centers can significantly impact the photocatalytic performance of OCPs. PC-PT with an ionic P(Me)-center exhibits a HER up to 2050 μmol h^{-1} g^{-1} under visible light. Overall, the current study not only paves the way to explore a new polymerization protocol for constructing organophosphorus polymeric networks with better-controlled and well-defined chemical structures, but also provides a new strategy to fine-tune the photocatalytic H_2 production performance of OCPs.

Data availability

The ESI† includes all experimental details, including synthesis and characterization of all products reported in this study, theoretical calculation, solid-state NMR experiments, FTIR experiments, XPS experiments, Mott–Schottky experiments, TGA experiments, contact angle experiments, and NMR spectra of all products are included as well.

Author contributions

All authors have given approval to the final version of the manuscript.

Conflicts of interest

The authors declare the following competing financial interest: parts of the results have been filed in a patent where Y. Ren and Z. Zhang are the inventors.

Acknowledgements

This research was financially supported by ShanghaiTech University start-up funding and the Natural Science Foundation

of Shanghai (19ZR1433700). The authors also acknowledge the support from Analytical Instrumentation Center (SPST-AIC10112914), SPST, ShanghaiTech University and the HPC Platform of ShanghaiTech University for providing resources and computing time. The authors thank Prof. Z. Wei for the helpful discussion on the computational studies. The authors also thank Y.-F. Liu for assistance in contact angle measurements.

Notes and references

1 P. M. Beaujuge and J. R. Reynolds, *Chem. Rev.*, 2010, **110**, 268–320.
2 N. Chaoui, M. Trunk, R. Dawson, J. Schmidt and A. Thomas, *Chem. Soc. Rev.*, 2017, **46**, 3302–3321.
3 I. B. Dimov, M. M. Moser, G. G. Malliaras and I. McCulloch, *Chem. Rev.*, 2022, **122**, 4356–4396.
4 J. M. Lee and A. I. Cooper, *Chem. Rev.*, 2018, **118**, 4731–4816.
5 J. G. Ibanez, M. E. Rincon, S. Gutierrez-Granados, M. Chahma, O. A. Jaramillo-Quitero and B. A. Frontana-Uribe, *Chem. Rev.*, 2020, **120**, 2171–2214.
6 Z. Zhang, J. Jia, Y. Zhi, S. Ma and X. Liu, *Chem. Soc. Rev.*, 2022, **51**, 2444–2490.
7 H. Yao, L. Ye, H. Zhang, S. Li, S. Zhang and J. Hou, *Chem. Rev.*, 2016, **116**, 7397–7457.
8 A. Natansohn and P. Rochon, *Chem. Rev.*, 2002, **102**, 4139–4176.
9 J. Liu, J. W. Lam and B. Z. Tang, *Chem. Rev.*, 2009, **109**, 5799–5867.
10 S. E. Root, S. Savagatrup, A. D. Printz, D. Rodriquez and D. J. Lipomi, *Chem. Rev.*, 2017, **117**, 6467–6499.
11 L. Dou, Y. Liu, Z. Hong, G. Li and Y. Yang, *Chem. Rev.*, 2015, **115**, 12633–12665.
12 F. Jäkle, *Chem. Rev.*, 2010, **110**, 3985–4022.
13 Z. Zhang, Q. Wang, H. Liu, T. Li and Y. Ren, *J. Am. Chem. Soc.*, 2022, **144**, 11748–11756.
14 J. A. L. Wells and A. Orthaber, Organophosphorus and Related Group 15 Polymers, in *Reference Module in Chemistry. Molecular Sciences and Chemical Engineering*, Elsevier, 2021.
15 R. C. So and A. C. Carreon-Asok, *Chem. Rev.*, 2019, **119**, 11442–11509.
16 H.-Y. Chen, J. Hou, A. E. Hayden, H. Yang, K. N. Houk and Y. Yang, *Adv. Mater.*, 2010, **22**, 371–375.
17 C.-H. Tsai, A. Fortney, Y. Qiu, R. R. Gil, D. Yaron, T. Kowalewski and K. J. T. Noonan, *J. Am. Chem. Soc.*, 2016, **138**, 6798–6804.
18 X. Liu, Y. Xu and D. Jiang, *J. Am. Chem. Soc.*, 2012, **134**, 8738–8741.
19 B. Meng, Y. Ren, J. Liu, F. Jäkle and L. Wang, *Angew. Chem., Int. Ed.*, 2018, **57**, 2183–2187.
20 C. Xue, M. Peng, Z. Zhang, X. Han, Q. Wang, C. Li, H. Liu, T. Li, N. Yu and Y. Ren, *Macromolecules*, 2022, **55**, 3850–3859.
21 X. Yin, J. Chen, R. A. Lalancette, T. B. Marder and F. Jäkle, *Angew. Chem., Int. Ed.*, 2014, **53**, 9761–9765.
22 R. Zhao, C. Dou, Z. Xie, J. Liu and L. Wang, *Angew. Chem., Int. Ed.*, 2016, **55**, 5313–5317.
23 X. Wang, L. Chen, S. Y. Chong, M. A. Little, Y. Wu, W. H. Zhu, R. Clowes, Y. Yan, M. A. Zwijnenburg, R. S. Sprick and A. I. Cooper, *Nat. Chem.*, 2018, **10**, 1180–1189.
24 C. Han, P. Dong, H. Tang, P. Zheng, C. Zhang, F. Wang, F. Huang and J. X. Jiang, *Chem. Sci.*, 2020, **12**, 1796–1802.
25 Z. J. Wang, X. Y. Yang, T. J. Yang, Y. B. Zhao, F. Wang, Y. Chen, J. H. Zeng, C. Yan, F. Huang and J. X. Jiang, *ACS Catal.*, 2018, **8**, 8590–8596.
26 M. Sachs, R. S. Sprick, D. Pearce, S. A. J. Hillman, A. Monti, A. A. Y. Guilbert, N. J. Brownbill, S. Dimitrov, X. Y. Shi, F. Blanc, A. M. Zwijnenburg, J. Nelson, J. R. Durrant and A. I. Cooper, *Nat. Commun.*, 2018, **9**, 4968.
27 J. B. Rodriguez and C. Gallo-Rodriguez, *ChemMedChem*, 2019, **14**, 190–216.
28 P. Seweryn, L. B. Van, M. Kjeldgaard, C. J. Russo, L. A. Passmore, B. Hove-Jensen, B. Jochimsen and D. E. Brodersen, *Nature*, 2015, **525**, 68–72.
29 H. Fernández-Pérez, P. Etayo, A. Panossian and A. Vidal-Ferran, *Chem. Rev.*, 2011, **111**, 2119–2176.
30 D. A. DiRocco, Y. Ji, E. C. Sherer, A. Klapars, M. Reibarkh, J. Dropinski, R. Mathew, P. Maligres, A. M. Hyde, J. Limanto, A. Brunskill, R. T. Ruck, L.-C. Campeau and I. W. Davies, *Science*, 2017, **356**, 426–430.
31 K. Wu and A. G. Doyle, *Nat. Chem.*, 2017, **9**, 779–784.
32 M. C. Hilton, X. Zhang, B. T. Boyle, J. V. Alegre-Requena, R. S. Paton and A. McNally, *Science*, 2018, **362**, 799–804.
33 X. Zhang, K. G. Nottingham, C. Patel, J. V. Alegre-Requena, J. N. Levy, R. S. Paton and A. McNally, *Nature*, 2021, **594**, 217–222.
34 M. Hirai, N. Tanaka, M. Sakai and S. Yamaguchi, *Chem. Rev.*, 2019, **119**, 8291–8331.
35 T. Baumgartner, *Acc. Chem. Res.*, 2014, **47**, 1613–1622.
36 F. Vidal and F. Jäkle, *Angew. Chem., Int. Ed.*, 2019, **58**, 5846–5870.
37 Q. Zhang, S. Zhang and S. Li, *Macromolecules*, 2012, **45**, 2981–2988.
38 S. Fischer, A. Schimanowitz, R. Dawson, I. Senkovsk, S. Kaskel and A. Thomas, *J. Mater. Chem. A*, 2014, **2**, 11825–11829.
39 K. H. Park, Y. J. Kim, G. B. Lee, T. K. An, C. E. Park, S.-K. Kwon and Y.-H. Kim, *Adv. Funct. Mater.*, 2015, **25**, 3991–3997.
40 H. K. Mackenzie, B. W. Rawe, K. Samedov, H. T. G. Walsgrove, A. Uva, Z. Han and D. P. Gates, *J. Am. Chem. Soc.*, 2020, **142**, 10319–10324.
41 K. M. Korch and D. A. Watson, *Chem. Rev.*, 2019, **119**, 8192–8228.
42 I. Wauters, W. Debrouwer and C. V. Stevens, *Beilstein J. Org. Chem.*, 2014, **10**, 1064–1096.
43 I. P. Beletskaya, V. V. Afanasiev, M. A. Kazankova and I. V. Efimova, *Org. Lett.*, 2003, **5**, 4309–4311.
44 A. A. Zagidullin, I. F. Sakhapov, V. A. Miluykov and D. G. Yakhvarov, *Molecules*, 2021, **26**, 5283.
45 V. V. Afanasiev, I. P. Beletskaya, M. A. Kazankova, I. V. Efimova and M. U. Antipin, *Synthesis*, 2003, **18**, 2835–2838.

46 B. Carsten, F. He, H. J. Son, T. Xu and L. Yu, *Chem. Rev.*, 2011, **111**, 1493–1528.
47 A. K. Leone and A. J. McNeil, *Acc. Chem. Res.*, 2016, **49**, 2822–2831.
48 B. Ma, Q. Shi, X. Ma, Y. Li, H. Chen, K. Wen, R. Zhao, F. Zhang, Y. Lin, Z. Wang and H. Huang, *Angew. Chem., Int. Ed.*, 2033, **61**, e202115969.
49 N. A. Kukhta, A. Marks and C. K. Luscombe, *Chem. Rev.*, 2022, **122**, 4325–4355.
50 H.-A. Ho, A. Najari and M. Leclerc, *Acc. Chem. Res.*, 2008, **41**, 168–178.
51 C. Cordovilla, C. Bartolomé, J. M. Martínez-Ilarduya and P. Espinet, *ACS Catal.*, 2015, **5**, 3040–3053.
52 P. Espinet and A. M. Echavarren, *Angew. Chem., Int. Ed.*, 2004, **43**, 4704–4734.
53 A. Ariafard and B. F. Yates, *J. Am. Chem. Soc.*, 2009, **131**, 13981–13991.
54 A. L. Casado and P. Espinet, *J. Am. Chem. Soc.*, 1998, **120**, 8978–8985.
55 K. Takeuchi, K.-W. Kim, Y.-J. Kim, N. Fukaya, K. Sato and J.-C. Choi, *ACS Omega*, 2020, **5**, 29706–29713.
56 D. L. Crossley, J. Cid, L. D. Curless, M. L. Turner and M. J. Ingleson, *Organometallics*, 2015, **34**, 5767–5774.
57 A. Lik, L. Fritze, L. Müller and H. Helten, *J. Am. Chem. Soc.*, 2017, **139**, 5692–5695.
58 S. E. Tunney and J. K. Stille, *J. Org. Chem.*, 1987, **52**, 748–753.
59 J. Fritsch, F. Drache, G. Nickerl, W. Böhlmann and S. Kaskel, *Microporous Mesoporous Mater.*, 2013, **172**, 167–173.
60 Z. Yang, Z. Zhang, X. Xue, K. Yang, R. Gao, N. Yu and Y. Ren, *Phys. Chem. Chem. Phys.*, 2021, **23**, 24265–24272.
61 Y. Wang, A. Vogel, M. Sachs, R. S. Sprick, L. Wilbraham, S. J. A. Moniz, R. Godin, M. A. Zwijnenburg, J. R. Durrant, A. I. Cooper and J. Tang, *Nat. Energy*, 2019, 746–760.
62 Y. Bai, L. Wilbraham, B. J. Slater, M. A. Zwijnenburg, R. S. Sprick and A. I. Cooper, *J. Am. Chem. Soc.*, 2019, **141**, 9063–9071.
63 J. Huang, J. Tarubek, R. Kulkarni, C. Wang, M. Dračínský, G. J. Smales, Y. Tian, S. Ren, B. R. Pauw, U. Resch-Genger and M. J. Bojdys, *Chem. – Eur. J.*, 2019, **25**, 12342–12348.
64 R. S. Sprick, C. M. Aitchison, E. Berardo, L. Turcani, L. Wilbraham, B. M. Alston, K. E. Jelfs, M. A. Zwijnenburg and A. I. Cooper, *J. Mater. Chem. A*, 2018, **6**, 11994–12003.
65 C. Zhao, Z. Chen, R. Shi, X. Yang and T. Zhang, *Adv. Mater.*, 2020, **32**, 1907296.
66 B. He, S. Zhang, Y. Zhang, G. Li, B. Zhang, W. Ma, B. Rao, R. Song, L. Zhang, Y. Zhang and G. He, *J. Am. Chem. Soc.*, 2019, **141**, 9063–9071.
67 Z. Wang, X. Yang, T. Yang, Y. Zhao, F. Wang, Y. Chen, J. H. Zeng, C. Yan, F. Huang and J.-X. Jiang, *ACS Catal.*, 2018, **8**, 8590–8596.
68 R. S. Sprick, B. Bonillo, R. Clowes, P. Cuiglion, N. J. Brownbill, B. J. Slater, F. Blanc, M. A. Zwijnenburg, D. J. Adam and A. I. Cooper, *Angew. Chem., Int. Ed.*, 2016, **55**, 1792–1796.